

Elastic and quasi-elastic electron scattering on the $N = 14, 20,$ and 28 isotonic chains

Andrea Meucci, Matteo Vorabbi, Carlotta Giusti, and Franco Davide Pacati
*Dipartimento di Fisica, Università degli Studi di Pavia and
INFN, Sezione di Pavia, Via A. Bassi 6, I-27100 Pavia, Italy*

Paolo Finelli
*Dipartimento di Fisica e Astronomia, Università degli Studi di Bologna and
INFN, Sezione di Bologna, Via Irnerio 46, I-40126 Bologna, Italy*
(Dated: September 25, 2017)

We present theoretical predictions for electron scattering on the $N = 14, 20,$ and 28 isotonic chains from proton-deficient to proton-rich nuclei. The calculations are performed within the framework of the distorted-wave Born approximation and the proton and neutron density distributions are evaluated adopting a Relativistic Hartree-Bogoliubov (RHB) approach with a density dependent meson-exchange interaction. We present results for the elastic and quasi-elastic cross sections and for the parity-violating asymmetry parameter. Owing to the correlations between the evolution of the electric charge form factors along each chain with the underlying proton shell structure of the isotones, elastic electron scattering experiments on isotones can provide useful informations about the occupation and filling of the single-particle levels of protons.

PACS numbers: 25.30.Bf; 21.10.-k; 25.30.Fj; 24.10.Jv

Keywords: elastic electron scattering; Relativistic mean field models; Ground-state properties

I. INTRODUCTION

The study of nuclear properties has gained large and detailed information from reactions investigating the nuclear response to external probes [1–5]. Electron induced reactions are particularly well suited to explore such properties, as the predominant electromagnetic interaction of electrons with nuclei is well known and relatively weak. Electrons are able to penetrate nuclear matter deeply and without a large perturbation of the structure, being their mean free path in nuclei much larger than the nuclear dimensions. Moreover, as the energy ω and the momentum \mathbf{q} transferred to the nucleus can be varied independently, the obtained spectral function can be mapped with a resolution that is adjusted to the scale of the process that is considered. A lot of experimental and theoretical work on elastic and inelastic electron scattering at different energies has provided detailed information on the charge density distribution of the nuclear ground state and on the energy, strength, and quantum numbers of the excited states produced by single particle (s.p.) or collective excitation mechanisms [2, 6–8].

At a transferred energy of about $\omega = q^2/(2m_N)$, where m_N is the nucleon mass, the quasi-elastic (QE) peak appears. In this kinematic region the probe interacts essentially with one single nucleon which is then ejected and all the other nucleons behave as spectators. If only the scattered electron is detected, we have the inclusive reaction where all final nuclear states are included. A considerable number of data have been collected in the QE region [5, 9, 10], concerning not only the differential cross sections but also the separation of longitudinal and transverse response functions.

When also an emitted proton is detected in coincidence with the outgoing electron and the residual nucleus is left in a discrete eigenstate we have an exclusive reaction. A large number of coincidence ($e, e'p$) experiments have been performed, which have confirmed the assumption of a direct knockout mechanism and have provided detailed information on the s.p. properties of light-to-heavy nuclei [4, 9, 11–17]. In particular, the s.p. energies and the quantum numbers of the emitted nucleon inside the nucleus have been determined, directly relating to shell model properties. Moreover, the comparison between experimental data and theoretical calculations made it possible to extract spectroscopic factors, which revealed a partial occupation of the different shells and therefore the importance of nuclear correlations and the limits of a mean-field description of nuclear structure.

The use of electron scattering can be extended to the study of exotic nuclei far from stability line. The evolution of nuclear properties with the increasing asymmetry between the number of protons and neutrons is one of the most interesting topics of nuclear physics. Of particular interest is the behavior of the s.p. properties, with a consequent modification of the shell model magic numbers. The exclusive ($e, e'p$) reaction would be the best suited tool for this study [18, 19]. However, the measurement of ($e, e'p$) cross sections requires a double coincidence detection which is very difficult. Experiments for elastic scattering, and possibly inclusive QE scattering, appear easier to perform and are therefore to be considered as a first step.

In the next years radioactive ion beam (RIB) facilities [20–22] will produce a large amount of data on unstable nuclei. In particular, electron-RIB colliders using storage rings are under construction at RIKEN (Japan) [23–25] and GSI (Germany) [26]. Proposals have been presented for the ELISE experiment at FAIR in Germany [27–29] and the SCRIPT project in Japan [30, 31].

From the theoretical point of view, several studies of electron scattering on unstable nuclei have already been published [18, 19, 32–47]. In a recent paper [48] we have presented and discussed numerical predictions for elastic and inclusive QE electron scattering on oxygen and calcium isotopic chains, with the aim of investigating the evolution of some nuclear properties with increasing asymmetry between the number of neutrons and protons. The elastic electron scattering gives information on the global properties of a nucleus and, in particular, on the charge density distributions and on the properties of proton wave functions. The inclusive QE scattering is the integral of the spectral density function over all the available final states. As such, it is affected by the dynamical properties and preferably exploits the nuclear s.p. aspects.

It is much more difficult to measure neutron density distributions. Direct access to the neutron distribution can be obtained from the parity-violating asymmetry parameter A_{pv} , which is defined as the difference between the cross sections for the scattering of right- and left-handed longitudinally polarized electrons [49–51]. This quantity is related to the radius of the neutron distribution R_n , because Z^0 -boson exchange, which mediates the weak neutral interaction, couples mainly to neutrons and gives a model-independent measurement of R_n .

The first measurement of A_{pv} was performed by the PREX experiment [52, 53] on ^{208}Pb with a poor resolution. More stringent results are expected from an improved experiment (PREX-II [54]) which has been recently approved. A recent result for the neutron skin on ^{208}Pb has been extracted from coherent pion photoproduction cross sections measured at MAMI Mainz electron microtron [55]. These data, combined with the results of the CREX experiment on ^{48}Ca [56], which has also been conditionally approved, will provide an important test on the validity of microscopic models concerning the dependence of R_n on the mass number A and the properties of the neutron skin.

In [48] we have compared our calculations for the asymmetry parameter A_{pv} with the result of the first PREX experiment on ^{208}Pb and have obtained a good agreement with the empirical value. Moreover, we have provided numerical predictions for the future experiment CREX on ^{48}Ca and we have studied the behavior of A_{pv} along oxygen

and calcium isotonic chains.

In this work we extend our study to isotonic chains. We present and discuss numerical predictions for the cross sections of elastic and inclusive QE electron scattering and for the parity-violating asymmetry parameter A_{pv} on the $N = 14, 20,$ and 28 isotonic chains. This is complementary to our previous study on isotopic chains of [48]. Electron scattering on an isotopic chain gives information on the dependence of the charge density distribution and of the proton wave functions on the neutron number. In an isotonic chain we can investigate the behavior of the charge distribution and of the proton s.p. states when a new proton is added to the nucleus. Nuclei with both neutron and proton excess are considered in our study. Our choice of the isotonic chains is motivated by the fact that data for light nuclei, such as those with $N = 14$, are likely to be obtained in future electron scattering facilities such as SCRIT and ELISE; the $N = 20,$ and 28 isotonic chains correspond to nuclei with an intermediate mass and a magic number of neutrons. Medium-size nuclei are very interesting to study the details of nuclear forces. In particular, semi-magic $N = 20$ and 28 isotones are composed by a moderately large number of nucleons with orbits clearly separated from the neighboring ones, so that smooth but continuous modifications in nuclear shapes can be observed when protons are added or removed. Therefore, the peculiar features of nuclear forces between nucleons moving in orbits with specific quantum numbers are much easier to disentangle in medium than in heavy nuclei, where the modification of shell structures occurs only when many nucleons are involved. A recent review of the evolution of the $N = 28$ shell closure far from stability can be found in [57].

The basic ingredients of the calculations for both elastic and QE scattering are the ground state wave functions of proton and neutron s.p. states. Models based on the relativistic mean-field (RMF) approximation have been successfully applied in analyses of nuclear structure from light to superheavy nuclei. RMF models are phenomenological because the parameters of their effective Lagrangian are adjusted to reproduce the nuclear matter equation of state and a set of global properties of spherical closed-shell nuclei [58–61]. In recent years effective hadron field theories with additional non-linear terms and density-dependent coupling constants adjusted to Dirac-Brueckner self-energies in nuclear matter have been able to obtain a satisfactory nuclear matter equation of state and to reproduce the empirical bulk properties of finite nuclei [62]. To obtain a proper description of open-shell nuclei a unified and self-consistent treatment of mean-field and pairing correlations is necessary. The relativistic Hartree-Bogoliubov (RHB) model provides a unified treatment of the nuclear mean-field and pairing correlations, which is crucial for an accurate description of the properties of the ground and excited states in weakly bound nuclei, and has been successfully employed in the analyses of exotic nuclei far from the valley of stability. For most nuclei here considered, however, pairing effects are negligible or small and the RHB model gives wave functions practically equivalent to the ones that can be obtained with the relativistic Dirac-Hartree model used in [48].

The cross sections for elastic electron scattering are obtained solving the partial wave Dirac equation and include Coulomb distortion effects. For the inclusive QE electron scattering calculations are performed with the relativistic Green's function (RGF) model, which has already been widely and successfully applied to the analysis of QE electron and neutrino-nucleus scattering data on different nuclei [63–70].

The paper is organized as follows. In Sec. II we give the main ingredients of the relativistic model for the calculation of the ground state observables. In Sec. III we outline the main features of the elastic electron scattering, including the definition of the parity-violating asymmetry. The results for elastic electron scattering on the $N = 28, 20,$ and 14 isotonic chains are presented and discussed in Sec. IV. In Sec. V we present the inclusive QE scattering and show and discuss the corresponding numerical results. Some conclusions are drawn in Sec. VI.

II. RELATIVISTIC MODEL FOR GROUND STATE OBSERVABLES

The RHB model [62] represents the most sophisticated method to include particle-hole (ph) and particle-particle (pp) interactions in a mean-field approximation. In this framework, the ground state of a nucleus $|\Phi_0\rangle$ is represented by the product of independent single-quasiparticle states that are eigenvectors of a Hamiltonian containing two average potentials: a self-consistent mean-field \hat{h} , which encloses all the long range ph correlations, and a pairing field $\hat{\Delta}$, which includes pp correlations. For the ph part we use a finite range model in which the nuclear interaction is mediated by meson exchange [58]. This effective interaction is characterized by meson masses and density dependent coupling constants. Even if recently there have been some improvements [71, 72] towards an ab-initio derivation, the most successful parametrizations are purely phenomenological with parameters adjusted to reproduce the nuclear matter equation of state and a set of bulk properties of closed-shell nuclei (we employed a DDME1 parameterization [73]). On the other hand, pairing correlations are described by the corresponding pp -part of the finite range Gogny interaction [74, 75]. The pairing interaction is treated at a non relativistic level, as discussed in [76].

The relativistic Hartree-Bogoliubov equations can be written as follows

$$\begin{pmatrix} \hat{h} - m - \lambda & \hat{\Delta} \\ -\hat{\Delta}^* & -\hat{h} + m + \lambda \end{pmatrix} \begin{pmatrix} U(r) \\ V(r) \end{pmatrix} = E \begin{pmatrix} U(r) \\ V(r) \end{pmatrix}, \quad (1)$$

where m is the nucleon mass and λ is the chemical potential determined by the particle number condition. The column vectors denote the quasiparticle wave functions and E are the quasiparticle energies. The RHB equations are solved self-consistently, together with the Klein-Gordon equations for the meson fields and the Poisson equation for the photon field. The relevant density for electron scattering calculations is defined as follows

$$\rho_p(r) = \sum_{E_k > 0} V_k^\dagger \frac{1 - \tau_3}{2} V_k. \quad (2)$$

We refer the reader to [62] for more details.

III. ELASTIC ELECTRON SCATTERING

The differential cross section for the elastic scattering of an electron, with momentum transfer q , off a spherical spin-zero nucleus is given in the plane-wave Born approximation (PWBA) by

$$\left(\frac{d\sigma}{d\Omega'} \right)_{EL} = \sigma_M |F_p(q)|^2, \quad (3)$$

where Ω' is the scattered electron solid angle, σ_M is the Mott cross section [4, 9] and

$$F_p(q) = \int d\mathbf{r} j_0(qr) \rho_p(r) \quad (4)$$

is the charge form factor for a spherical nuclear charge density $\rho_p(r)$ and j_0 is the zeroth order spherical Bessel function.

In the case of medium and heavy nuclei the distortion produced on the electron wave functions by the nuclear Coulomb potential from $\rho_p(r)$ cannot be neglected and the elastic cross sections are obtained in the distorted-wave Born approximation (DWBA) from the numerical solution of the partial wave Dirac equation.

Our DWBA results are compared with the experimental differential cross sections for elastic electron scattering on four calcium isotopes ($^{40,42,44,48}\text{Ca}$) at an electron energy $\varepsilon = 250$ MeV in Fig. 1 and on $^{50,52,54}\text{Cr}$ at $\varepsilon = 200$ MeV and ^{48}Ti at $\varepsilon = 250$ MeV in Fig. 2. The DWBA calculations are able to reproduce the general trend of the data and give a good description of the experimental cross sections considered, except for small discrepancies at large scattering angles.

Another interesting quantity that can be measured in elastic electron scattering is the parity-violating asymmetry, which is defined as the difference between the cross sections for the elastic scattering of electrons longitudinally polarized parallel and antiparallel to their momentum. This difference arises from the interference between photon and Z^0 exchange and represents an almost direct measurement of the Fourier transform of the neutron density [49, 79]. In fact, in Born approximation, neglecting strangeness contributions and the electric neutron form factor, the parity-violating asymmetry can be expressed as [80, 81]

$$A_{pv} = \frac{G_F q^2}{4\sqrt{2} \pi \alpha} \left[4 \sin^2 \Theta_W - 1 + \frac{F_n(q)}{F_p(q)} \right], \quad (5)$$

where $G_F \simeq 1.16639 \times 10^{-11}$ MeV $^{-2}$ is the Fermi constant and $\sin^2 \Theta_W \simeq 0.23$ is the Weinberg angle. Since $4 \sin^2 \Theta_W - 1$ is small and the proton form factor $F_p(q)$ is known, we see that A_{pv} provides a practical method to measure the neutron form factor $F_n(q)$ and hence the neutron radius. For these reasons parity-violating electron scattering (PVES) has been suggested as a clean and powerful tool for measuring the spatial distribution of neutrons in nuclei.

The first measurement of A_{pv} in the elastic scattering of polarized electrons from ^{208}Pb has been performed in Hall A at the Jefferson Lab (experiment PREX) [52, 53]. Another experiment with improved electronics (PREX-II) [54] has been recently approved. In addition, the experiment CREX [56], with the goal of measuring the neutron skin of ^{48}Ca , has also been conditionally approved.

Our DWBA results are in good agreement with the parameter A_{pv} measured by the first experiment PREX. The comparison can be found in [48], where our numerical predictions for the experiment CREX are also given.

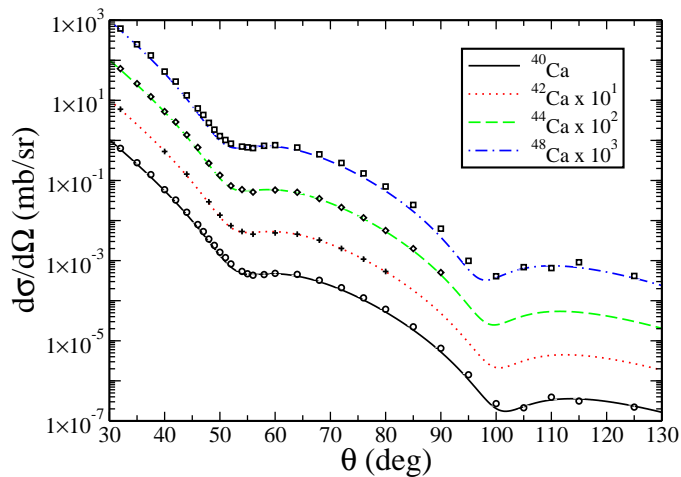


Figure 1. (Color online) Differential cross sections for elastic electron scattering on calcium isotopes at an electron energy $\varepsilon = 250$ MeV as functions of the scattering angle θ . Experimental data from [77].

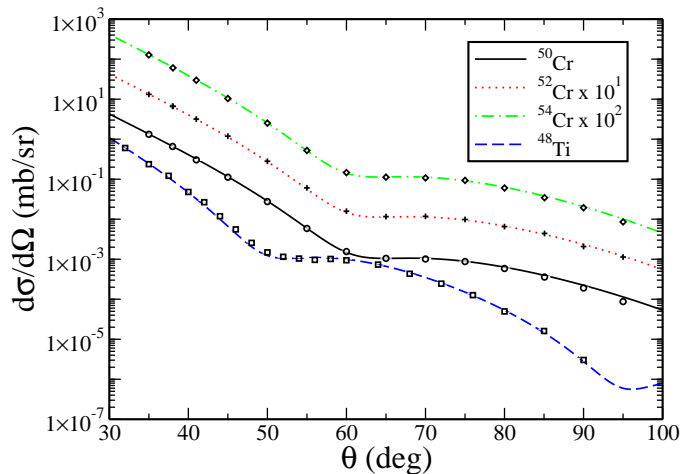


Figure 2. (Color online) Differential cross sections for elastic electron scattering on $^{50,52,54}\text{Cr}$ at $\varepsilon = 200$ MeV and ^{48}Ti at $\varepsilon = 250$ MeV as functions of θ . Experimental data from [77] (^{48}Ti) and [78] ($^{50,52,54}\text{Cr}$).

IV. RESULTS FOR ELASTIC ELECTRON SCATTERING ON THE $N = 28, 20$ AND 14 ISOTONIC CHAINS

In this Section we present our results for the evolution of some well-established observables in elastic electron scattering on the $N = 28, 20$ and 14 isotonic chains. Many of these nuclei lie in the region of the nuclear chart that is likely to be explored in future electron-scattering experiments. We first consider $N = 28$, then we extend our analysis to $N = 20$ and 14.

A. Results for $N = 28$

In panel (a) of Fig. 3 we plot the proton density distributions ρ_p as functions of the radial coordinate r along the $N = 28$ isotonic chain. These density distributions are obtained summing the squared moduli of the s.p. wavefunctions described in Section II. All the nuclei that we consider result to be bound but, experimentally, there are proton-deficient nuclei (from ^{40}Mg to ^{46}Ar), stable nuclei (from ^{48}Ca to ^{54}Fe) and one proton-rich nucleus (^{56}Ni).

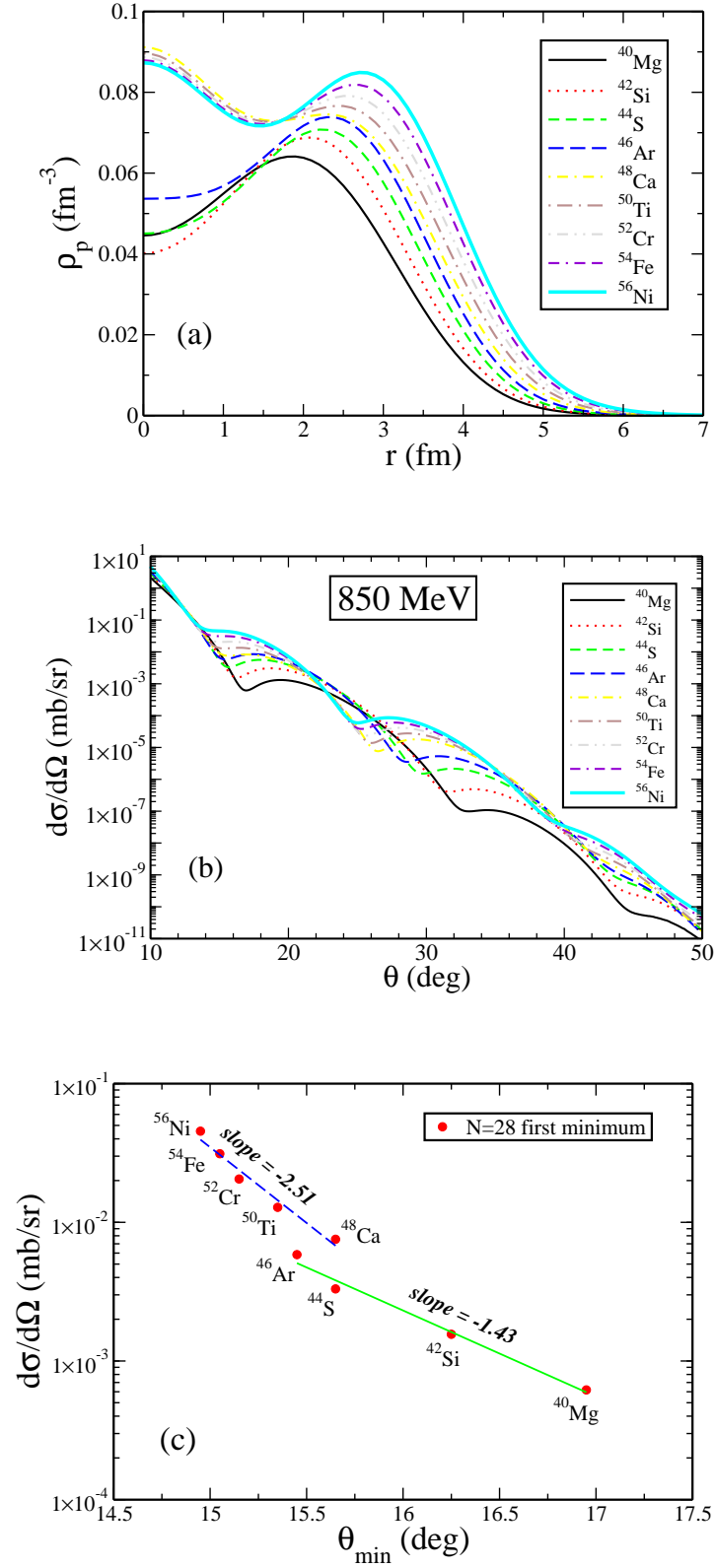


Figure 3. (Color online) Panel (a): proton distributions along the $N = 28$ isotonic chain. Panel (b): differential cross sections for elastic electron scattering at $\varepsilon = 850$ MeV as functions of θ . Panel (c): evolution of the first minimum of the differential cross section with the scattering angle θ .

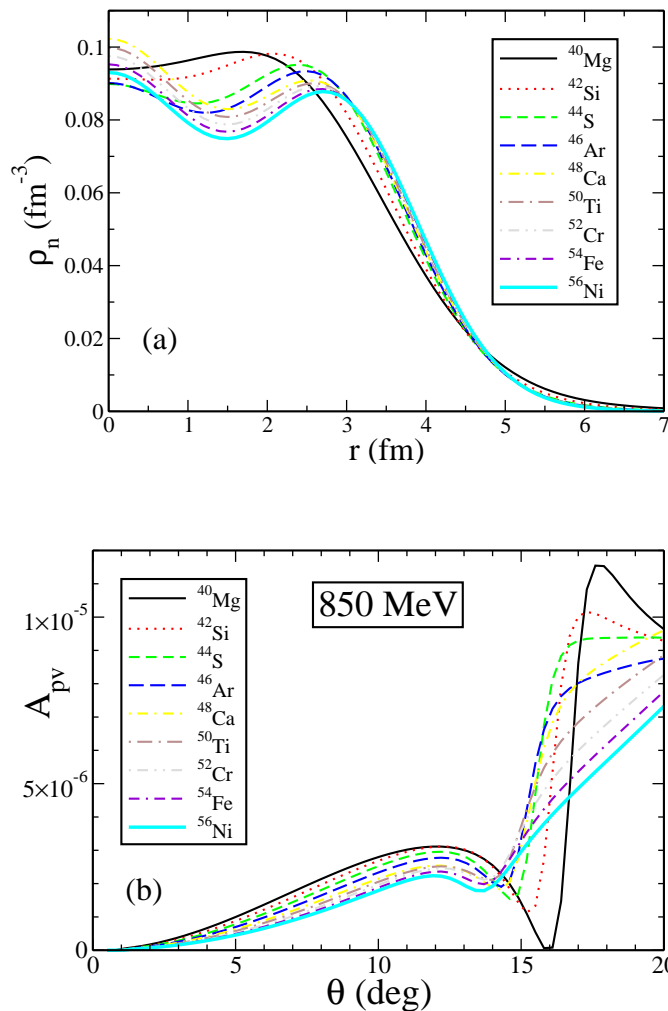


Figure 4. (Color online) Panel (a): neutron distributions along the $N = 28$ isotonic chain. Panel (b): parity-violating asymmetry parameters A_{pv} for elastic electron scattering at $\varepsilon = 850$ MeV as functions of the scattering angle θ .

The most significant effect of adding protons is to populate and extend the proton densities.

The differences of the proton density profiles in the nuclear interior display pronounced shell effects; the most relevant proton s.p. levels in our analysis of the $N = 28$ chain are the $2s_{1/2}$ and the $1f_{7/2}$. In the case of the heavier nuclei, starting from ^{48}Ca up to ^{56}Ni , we obtain similar results for ρ_p in the central region whereas the differences at large r can be ascribed to the filling of the $1f_{7/2}$ shell which starts from ^{50}Ti .

The proton density of the proton-deficient ^{46}Ar nucleus also gets a non negligible contribution from the $2s_{1/2}$ shell, which has an occupation number of 0.330, and, as a consequence, in the central region it is approximately 20% larger than those of lighter isotones. In our model the ^{42}Si nucleus, with 14 protons, behaves like a magical nucleus and its proton density does not get any contribution from neither the $2s_{1/2}$ nor the $1d_{3/2}$ shells which, on the contrary, contribute to ^{40}Mg and to ^{44}S densities which are, therefore, larger in the central region. However, the experimental evidence of a 2^+_1 state at 770 ± 19 keV [82], much smaller than for other nuclei in this chain, has been interpreted as a signal of the disappearance of the $N = 28$ shell closure around ^{42}Si and has suggested that proton-core excitations and the tensor interactions cannot be neglected [57, 83].

In panel (b) of Fig. 3 we present the differential cross sections for elastic electron scattering at $\varepsilon = 850$ MeV as functions of the scattering angle θ . These cross sections have been calculated in the DWBA and with the self-consistent relativistic ground-state charge densities. Although Coulomb distortion is included in the calculations, the elastic cross sections are still related to the behavior of the corresponding proton charge density as in Eq. 3.

With increasing proton number along the chain the positions of the diffraction minima usually shift toward smaller

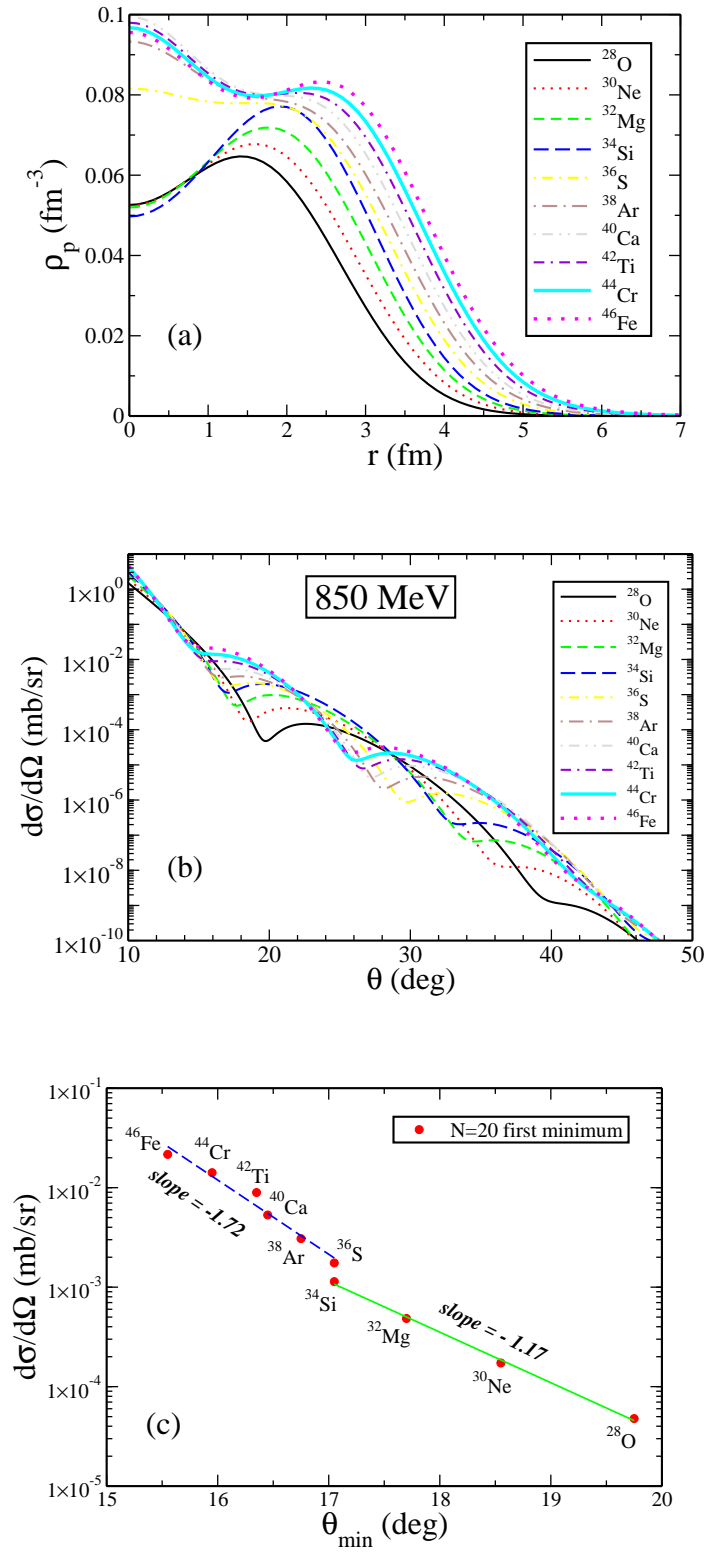


Figure 5. (Color online) The same as in Fig. 3 but for the $N = 20$ isotonic chain.

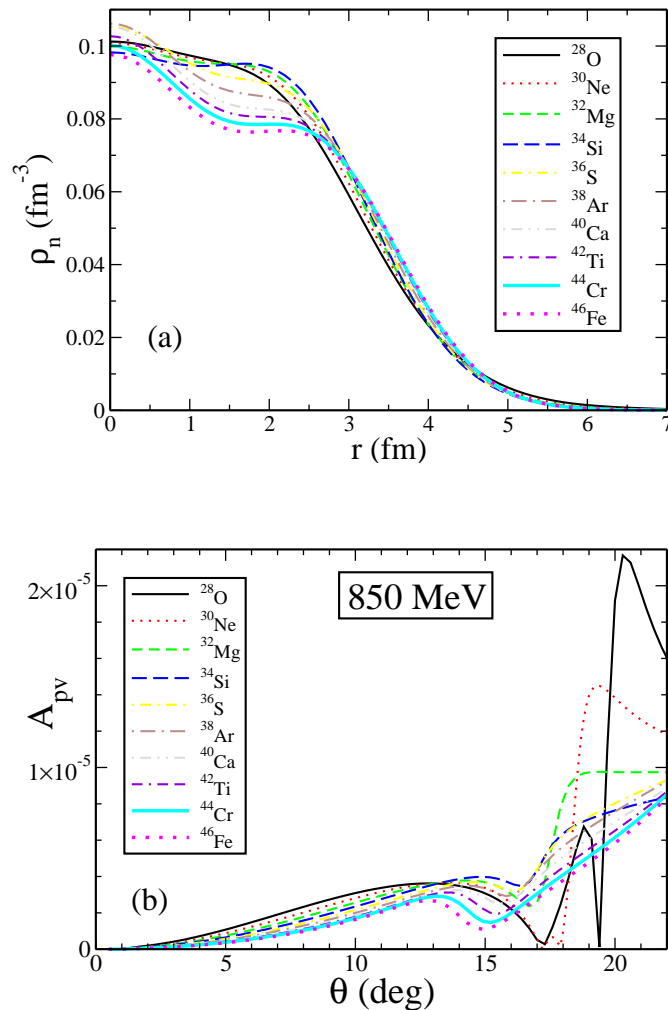


Figure 6. (Color online) The same as in Fig. 4 but for the $N = 20$ isotonic chain.

scattering angles, i.e., smaller values of the momentum transfer q . The shift of the minima is also accompanied by a simultaneous increase in the height of the corresponding maxima of the cross sections. The differential cross section provides information on the proton density distribution and we can look for possible correlations between the cross sections that can be directly related to the behavior of the proton distributions. In panel (c) of Fig. 3 we plot the evolution of the position of the first minimum of the elastic cross sections for each isotone in the chain. There is an evident transition between proton-poor and proton-rich isotones and it is not possible to fit the positions of the first minima with a straight line. In addition, the minimum for ^{48}Ca occurs at a larger scattering angle than for ^{46}Ar . However, it is still possible to draw a straight line that connects the minima for the lighter isotones up to ^{46}Ar and another line for the heavier isotones. The slope of the two lines are different. The isotones from ^{48}Ca up to ^{56}Ni have similar proton densities at small r and present only small differences at large r , which are ascribed to the filling of the $1f_{7/2}$ shell. In the case of the lighter isotones, we see that the ^{46}Ar and ^{44}S minima do not lie on the fitting lines. This is related to the non-negligible contribution of the proton in the $2s_{1/2}$ shell, which has occupation number 0.330 for ^{46}Ar and 0.153 for ^{44}S . The density of ^{40}Mg gets some small contribution from the $2s_{1/2}$ and the $1d_{3/2}$ shells but the minimum of its cross section is aligned with that of ^{42}Si .

The evolution of the neutron density distribution along an isotonic chain is less significant than that of the proton density distribution; generally, there is a decrease of the density in the nuclear interior and an extension toward large r to preserve the normalization to the constant number of neutrons, as it can be seen in panel (a) of Fig. 4. The cross sections for positive and negative helicity electron states at $\varepsilon = 850$ MeV have also been calculated and the resulting parity-violating asymmetry parameter A_{pv} is presented in panel (b) of Fig. 4 as a function of θ . In the case

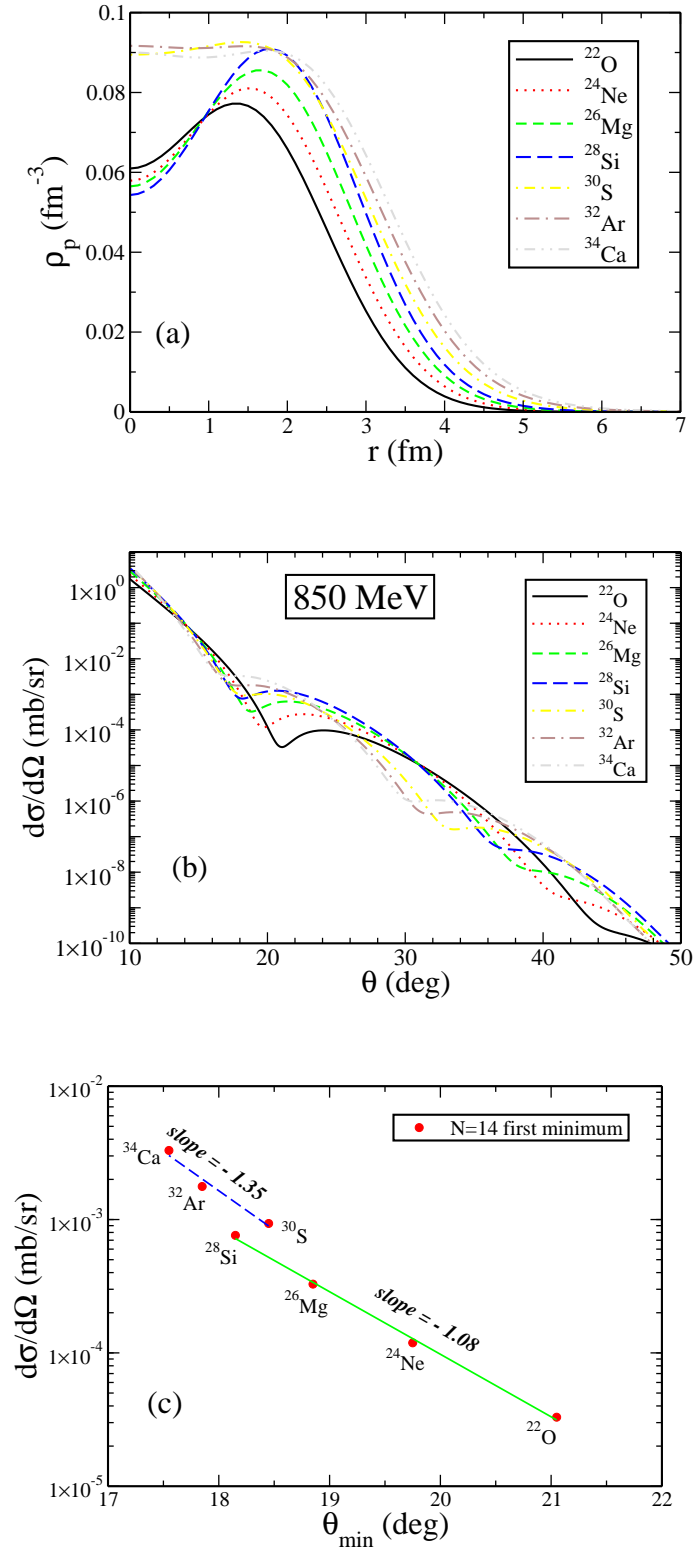


Figure 7. (Color online) The same as in Fig. 3 but for the $N = 14$ isotonic chain.

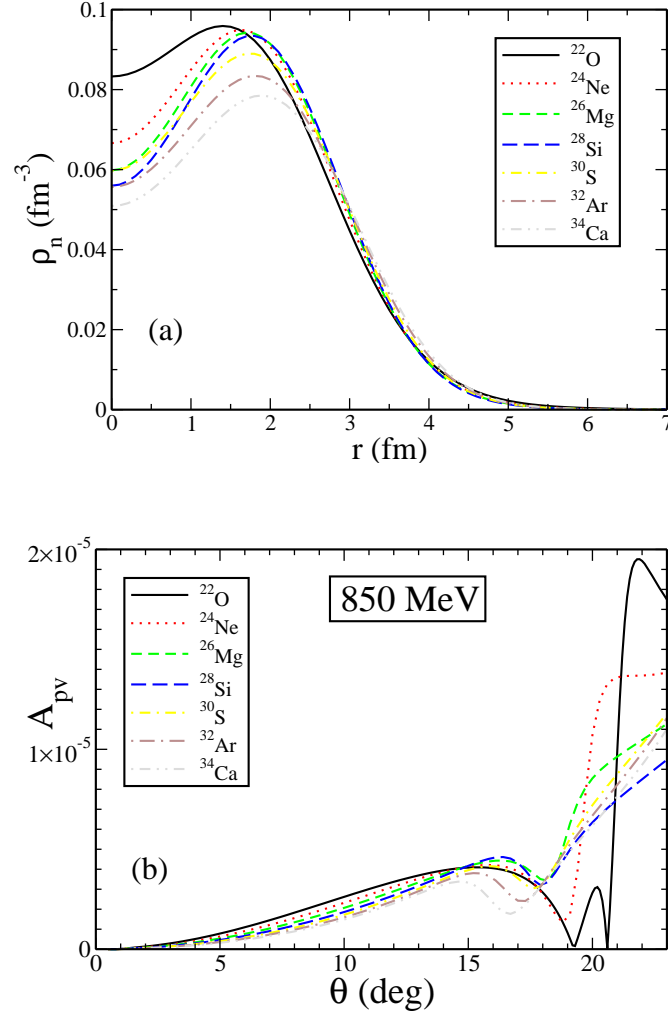


Figure 8. (Color online) The same as in Fig. 4 but for the $N = 14$ isotonic chain.

of oxygen and calcium isotopic chains we found that the evolution of the positions of the first minima as functions of the neutron excess is approximated by a linear fit [48]. In the case of the $N = 28$ isotones the position of the first minima of A_{pv} usually evolves toward smaller θ as the number of protons increases. However, ^{46}Ar and ^{48}Ca , as well as ^{50}Ti and ^{52}Cr , seem to have almost coincident minima. The value of A_{pv} at the minimum increases from ^{40}Mg to ^{46}Ar , then it decreases monotonically starting from ^{52}Cr .

B. Results for $N = 20$

In panel (a) of Fig. 5 we present our results for the proton density distributions as functions of r along the $N = 20$ isotonic chain. In our model all these nuclei result to be bound but, along this chain, there are proton-deficient nuclei (from ^{28}O to ^{34}Si), stable nuclei (^{36}S , ^{38}Ar , and ^{40}Ca) and proton-rich nuclei (^{42}Ti , ^{44}Cr , and ^{46}Fe). The densities of the proton-rich isotones are significantly extended toward larger r with respect to those of the proton-deficient ones. Also in this chain pronounced shell effects are visible in the nuclear interior. In particular, we find large differences in the radial profiles of the proton density of ^{34}Si and ^{36}S ; in our model the proton occupation number of the $2s_{1/2}$ shell of ^{36}S is not negligible and, owing to the observation that the squared wave function of the $2s_{1/2}$ state has a main peak at the center, the proton central density is enlarged. We obtain that also the proton occupation number of the $1d_{3/2}$ state for ^{36}S is significant; the corresponding peak of the squared wave function is away from the center and, therefore, the filling of the $1d_{3/2}$ state by protons increases the density away from the center. In the case of

the heavier nuclei, starting from ^{38}Ar up to ^{46}Fe , we obtain similar results for ρ_p in the central region, whereas the differences at large r can be ascribed to the addition of protons that populate and extend the densities.

In panel (b) of Fig. 5 we present the DWBA differential cross sections for elastic electron scattering at $\varepsilon = 850$ MeV as functions of the scattering angle θ . With increasing proton number along the chain the positions of the diffraction minima shift toward smaller scattering angles and, correspondingly, there is an increase in the height of the corresponding maxima of the cross sections. In panel (c) of Fig. 5 we plot the evolution of the position of the first minimum of the differential elastic cross section for each isotone in the chain. Owing to the large differences in the radial profiles of the densities of ^{34}Si and ^{36}S , it is not possible to fit the position of the first minima with a straight line. In addition, the minimum for ^{34}Si occurs at the same scattering angle as for ^{36}S . Also in this chain we can draw a straight line that connects the minima for the lighter isotones up to ^{34}Si and another line for the heavier isotones. The slope of the two lines is different.

Recently, there has been a significant interest in looking for “bubble” nuclei, i.e., nuclear systems where the central density is significantly reduced or vanishing with respect to the saturation density. Recent theoretical calculations, including RMF parametrizations [84–86] and Skyrme energy density functional [39, 40, 87], predict a central depletion of the charge density distributions for ^{34}Si and for some Ar isotopes but, usually, ^{34}Si is the only candidate for which the studies agree. However, a nuclear “bubble” has never been experimentally observed. In [88] the existence of a proton “bubble” structure in the low-lying excited 0_2^+ and 2_1^+ states of ^{34}Si is found to be very unlikely, owing to the results of a new RMF method which includes mixing of both particle-number and angular-momentum projected quadrupole deformed states. In panel (a) of Fig. 5 large differences can be seen between the proton density of ^{34}Si and ^{36}S . This result agrees with similar findings of other RMF models [84, 85]. In particular, as it is shown in panel (c) of Fig. 5, the positions of the first minima of the elastic cross sections of ^{34}Si and ^{36}S do not fall on the same straight line and this should provide a useful test that could be investigated at future electron scattering facilities.

In panel (a) of Fig. 6 we present the evolution of the neutron density distribution along the $N = 20$ isotonic chain. For the heavier isotones we observe a decrease of the density in the nuclear interior and a corresponding enhancement away from the center to preserve the normalization to the constant number of neutrons. In panel (b) of Fig. 6 we present the parity-violating asymmetry parameter A_{pv} as a function of θ evaluated at $\varepsilon = 850$ MeV. The neutron densities of ^{28}O and ^{30}Ne are very similar and their corresponding A_{pv} are almost coincident up to the first minimum. Starting from ^{32}Mg the minimum of A_{pv} shifts toward smaller angles.

C. Results for $N = 14$

In panel (a) of Fig. 7 we present our results for the proton density distributions as functions of r along the $N = 14$ isotonic chain. The densities in the nuclear interior of proton-deficient isotones up to the stable nucleus ^{28}Si are very similar. For all these nuclei only the two protons in the $1s_{1/2}$ state contribute to the density at the center. Starting from ^{30}S also the protons in the $2s_{1/2}$ state contribute and there is an evident transition in the density profile. As usual, the densities of the proton-rich isotones are significantly extended towards larger r with respect to those of the proton-deficient ones.

The DWBA differential cross sections for elastic electron scattering at $\varepsilon = 850$ MeV as functions of θ are displayed in panel (b) of Fig. 7. The positions of the diffraction minima shift toward smaller scattering angles as the proton number increases and, in addition, there is an enhancement in the height of the corresponding maxima of the cross sections. The evolution of the position of the first minimum of the differential cross section for each isotone in the chain, which is shown in panel (c) of Fig. 7, can adequately be described by the two different straight lines drawn in the figure, one connecting the minima of the lighter isotones up to ^{28}Si and the other one connecting the minima of the heavier isotones.

In panel (a) of Fig. 8 we present the evolution of the neutron density distribution along the $N = 14$ isotonic chain. The profiles of proton-deficient and proton-rich isotones are very different, in particular in the nuclear interior, but the normalization to the constant number of neutrons is always preserved. In panel (b) of Fig. 6 the parity-violating asymmetry parameter A_{pv} is presented as a function of θ . The neutron densities of ^{22}O and ^{24}Ne are very different from those of the other isotones in the chain and, as a consequence, their corresponding A_{pv} are very different. The position of the first minimum shifts toward smaller angles and the value of A_{pv} at the minimum increases from ^{22}O to ^{26}Mg , then it decreases starting from ^{28}Si .

V. INCLUSIVE QUASI-ELASTIC ELECTRON SCATTERING

The inclusive differential cross section for the quasi-elastic (QE) (e, e') scattering on a nucleus is obtained from the contraction between the lepton and hadron tensors as [9]

$$\left(\frac{d\sigma}{d\varepsilon' d\Omega'} \right)_{QE} = \sigma_M [v_L R_L + v_T R_T] , \quad (6)$$

where ε' is the energy of the scattered electron and the coefficients v come from the components of the lepton tensor that, under the assumption of the plane-wave approximation for the electron wave functions, depend only on the lepton kinematics [9]. All relevant nuclear structure information is contained in the longitudinal and transverse response functions R_L and R_T . The response functions can be expressed in terms of suitable linear combinations of the components of the hadron tensor, which are given by products of the matrix elements of the nuclear current between initial and final nuclear states.

In the QE region the nuclear response is dominated by one-nucleon processes where the scattering occurs with only one nucleon, which is subsequently emitted from the nucleus by a direct knockout mechanism, and the remaining nucleons behave as spectators. Therefore, QE electron scattering can adequately be described in the relativistic impulse approximation (RIA) by the sum of incoherent processes involving only one nucleon scattering and the components of the hadron tensor are obtained from the sum, over all the s.p. shell-model states, of the squared absolute value of the transition matrix elements of the single-nucleon current [9].

A reliable description of final-state interactions (FSI) between the emitted nucleon and the residual nucleus is a crucial ingredient for the description of (e, e') data. The relevance of final state interactions (FSI) has been clearly stated for the exclusive ($e, e'p$) reaction, where the use of a complex optical potential (OP) in the distorted-wave impulse approximation (DWIA) is required [4, 9, 15, 17, 18, 89–91]. The imaginary part of the OP produces an absorption that reduces the cross section and accounts for the loss of part of the incident flux in the elastically scattered beam to the inelastic channels which are open. In the inclusive scattering, where only the final lepton is detected and the final nuclear state is not determined, all elastic and inelastic channels contribute, all final-state channels should be retained and the flux, although redistributed among all possible channels, must be conserved.

In the relativistic plane-wave impulse approximation (RPWIA) FSI are simply neglected. In other approaches FSI are included in relativistic DWIA (RDWIA) calculations where the final nucleon state is evaluated with real potentials. In a different description of FSI relativistic Green's function (RGF) techniques [48, 63–67, 92–96] are used.

In the RGF model, under suitable approximations, which are basically related to the IA, the components of the nuclear response are written in terms of the single particle optical model Green's function; its spectral representation, that is based on a biorthogonal expansion in terms of a non-Hermitian optical potential \mathcal{H} and of its Hermitian conjugate \mathcal{H}^\dagger , is then exploited to obtain the components of the hadron tensor [63, 64] in terms of matrix elements of the same type as the DWIA ones of the exclusive ($e, e'p$) process, but involve eigenfunctions of both \mathcal{H} and \mathcal{H}^\dagger , where the imaginary part has an opposite sign and gives in one case a loss and in the other case a gain of strength. The RGF formalism allows us to reconstruct the flux lost into nonelastic channels in the case of the inclusive response starting from the complex OP which describes elastic nucleon-nucleus scattering data and to include contributions which are not included in other models based on the IA. Moreover, with the use of the same complex OP, it provides a consistent treatment of FSI in the exclusive and in the inclusive scattering. Because of the analyticity properties of the OP, the RGF model fulfills the Coulomb sum rule [63, 92, 97]. More details about the RGF model can be found in [48, 63–67, 92–96].

The RGF results can give a satisfactory description of experimental (e, e') cross sections in the QE region [48, 66]. In particular, the RGF provides a significant asymmetry in the scaling function, in agreement with the general behavior of electron scattering data that present a significant tail extended to large values of the transferred energy [98]. Moreover, the RGF results can describe the shape and the magnitude of charged-current QE neutrino-nucleus scattering MiniBooNE data [70] and of neutral-current elastic neutrino-nucleus MiniBooNE data [69]. Numerical predictions of the RGF model for the inclusive QE electron scattering on oxygen and calcium isotopic chains can be found in [48].

In the present calculations the s.p. bound nucleon states are obtained from the relativistic mean-field model described in Sect. II. The s.p. scattering states are eigenfunctions of the energy-dependent and A -dependent (A is the mass number) Democratic (DEM) parametrization for the relativistic optical potential (ROP) of [99], that is obtained through a fit of more than 200 data sets of elastic proton-nucleus scattering data on a wide range of nuclei which is not limited to doubly closed shell nuclei. The different number of protons along the isotonic chains produces different optical potentials (see [99] for more details). For the single-nucleon current we have adopted the relativistic free nucleon expression denoted as CC2 [63, 100].

The cross section of the inclusive QE (e, e') reaction along the $N = 28, 20$, and 14 isotonic chains at $\varepsilon = 1080$ MeV and $\theta = 32^\circ$ are shown in Fig. 9. In a first approximation we have neglected FSI and calculations have been performed

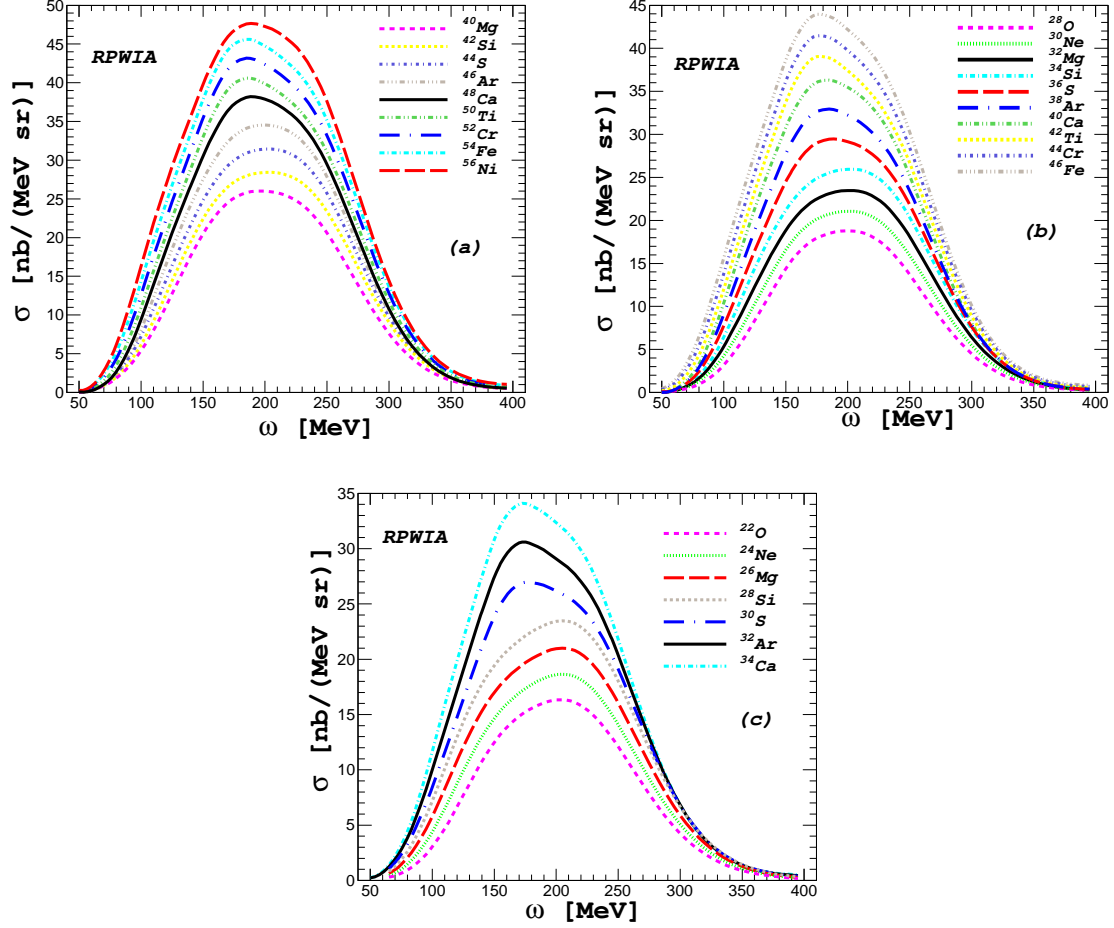


Figure 9. (Color online) Differential RPWIA cross sections for the inclusive QE (e, e') reaction on isotones with $N = 28, 20$, and 14 at $\varepsilon = 1080$ MeV and $\theta = 32^\circ$ as functions of the energy transfer ω .

in the RPWIA. In this approach the differences between the results for the various isotones are entirely due to the differences in the s.p. bound state wave functions of each isotone. While only the charge proton density distribution contributes to the cross section of elastic electron scattering, the cross section of QE electron scattering is obtained from the sum of all the integrated exclusive one-nucleon knockout processes, due to the interaction of the probe with all the individual nucleons, protons and neutrons, of the nucleus and contains information on the dynamics of the initial nuclear ground state. The main role is played by protons, which give most of the contribution. Increasing the proton number along each chain, owing to the enhancement of the proton contribution, there is a proportional increase of the QE cross sections. In contrast, no increase is found in the neutron contribution, which is less significant than the proton one. We can see in panel (b) of Fig. 9 that, even if the central density of ^{34}Si is reduced (see Fig. 5), the QE cross sections of ^{34}Si and ^{36}S do not show any significant difference that could be considered as a signal of “bubble” nuclei.

In Fig. 10 we show the QE (e, e') cross sections calculated in the RGF model for selected isotones of the $N = 28, 20$, and 14 chains in the same kinematics as in Fig. 9. The general trend of the cross sections, their magnitude, and their evolution with respect to the change of the proton number along each chain are generally similar in RPWIA and RGF. The RGF results are, however, somewhat larger. The FSI effects in the RGF calculations produce visible distortion effects: the RGF cross sections are not as symmetrical as the corresponding RPWIA ones and show a tail toward large values of the energy transferred ω that is related to the description of FSI with a complex energy-dependent ROP.

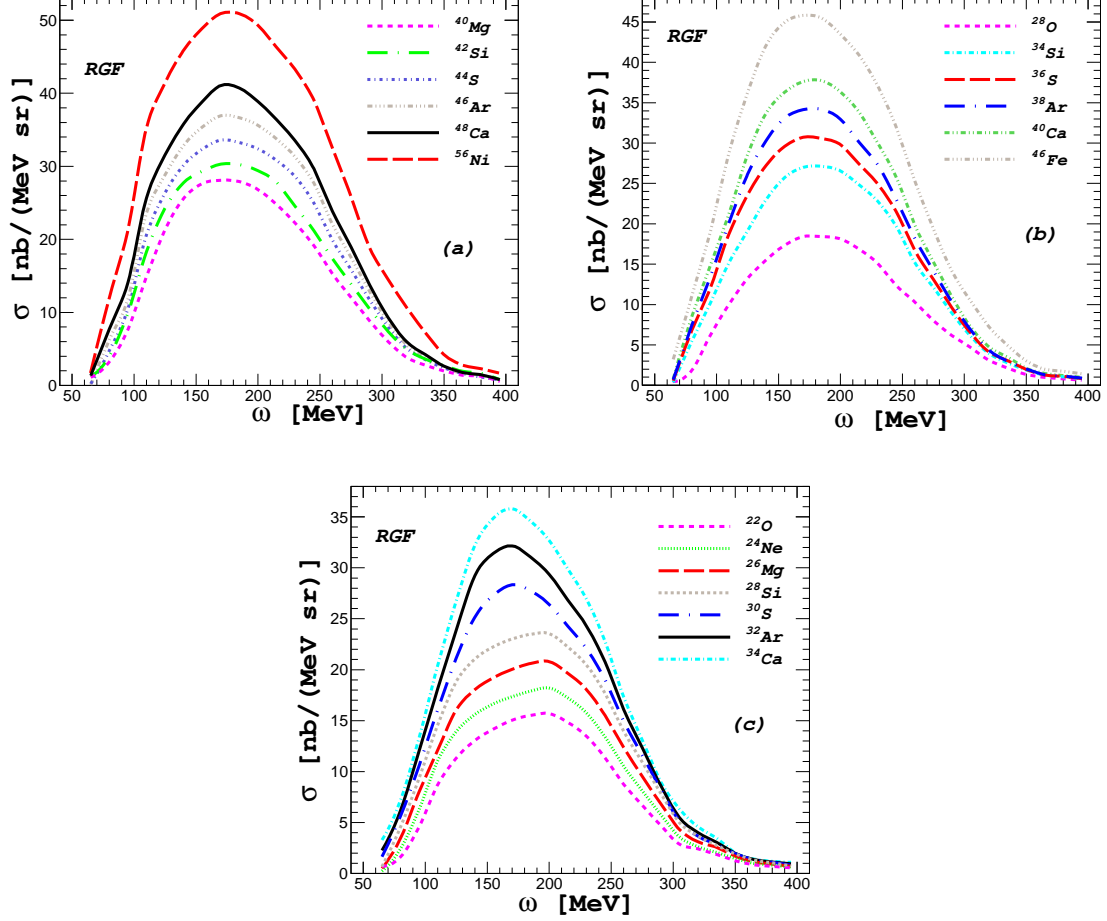


Figure 10. (Color online) Differential RGF cross sections for the inclusive QE (e, e') reaction on some selected isotones with $N = 28, 20$, and 14 at $\varepsilon = 1080$ MeV and $\theta = 32^\circ$ as functions of ω .

VI. SUMMARY AND CONCLUSIONS

We have presented and discussed numerical predictions for the cross section and the parity-violating asymmetry in elastic and quasi-elastic electron scattering on the $N = 28, 20$, and 14 isotonic chains with the aim to investigate their evolution with increasing proton number.

The understanding of the properties of nuclei far from the valley of stability is one of the major topic of interest in modern nuclear physics. Large efforts in this direction have been done over last years and are planned for the future in different laboratories worldwide. The use of electrons as probe provides a powerful tool to achieve this goal, owing to the fact that their interaction is well known and relatively weak with respect to the nuclear force and can therefore more adequately explore the details of inner nuclear structures. As a consequence of this weakness, the cross sections become very small and more difficult experiments have to be performed. The RIB facilities have opened the possibility to obtain unprecedented information into nuclear structures not available in nature but which are important in astrophysics and have a relevant role in the nucleosynthesis. Electron scattering experiments off exotic nuclei have been proposed in the ELISE experiment at FAIR and in the SCRIT project at RIKEN.

In this work both elastic and inclusive quasi-elastic electron scattering have been considered. The elastic scattering can give information on the global properties of nuclei and, in particular, on the different behavior of proton and neutron density distributions. The inclusive quasi-elastic scattering is affected by the dynamical properties and preferably exploits the single particle aspects of the nucleus. In addition, when combined with the exclusive ($e, e'p$) scattering, it is able to explore the evolution of the s.p. model with increasing asymmetry between the number of neutrons and protons. Many interesting phenomena are predicted in this situation: in particular, the modification of

the shell model magic numbers. A definite response can be obtained from the comparison with experimental data, which will discriminate between the different theoretical models, mainly referring to RMF approaches.

The calculations for the present investigation have been carried out within the RMF framework solving the relativistic Hartree-Bogoliubov equations starting from an effective interaction mediated by meson exchange. The calculated cross sections include both the hadronic and Coulomb final states interactions. The inclusive quasi-elastic scattering is calculated with the relativistic Green's function model, which conserves the global particle flux in all the final state channels, as it is required in an inclusive reaction.

The model has been compared with experimental data of elastic scattering already available on stable isotopes to check its reliability and subsequently applied to calculate elastic and inclusive quasi-elastic cross sections on the $N = 28, 20,$ and 14 isotonic chains. The possible disagreement of the experimental findings from the theoretical predictions will be a clear indication of the insurgence of new phenomena related to the proton to neutron asymmetry.

Our results show that the evolution of some specific observables can be useful to test shell effects related to the filling of s.p. orbits. The increase of the proton number along each chain essentially produces an enhancement and an extension of the proton densities. The densities of the proton-rich isotones are significantly extended toward larger r with respect to those of the proton-deficient ones. Pronounced shell effects are visible in the nuclear interior. The differential cross sections calculated for elastic electron scattering show that increasing proton number along an isotonic chain the positions of the diffraction minima generally shift toward smaller scattering angles, corresponding to lower values of the momentum transfer. The shift is accompanied by a simultaneous increase in the height of the corresponding maxima of the cross sections. A plot of the evolution of the position of the first minimum for each isotone in the chain shows a transition between proton-poor and proton-rich isotones. It is not possible to fit the positions of the first minima with a straight line, but it is possible to draw two straight lines, connecting the minima of the lighter and heavier isotones, with a different slope. This behavior has been found for all the three isotonic chains.

The neutron densities decrease in the nuclear interior and correspondingly increase away from the center to preserve the normalization to the constant number of neutrons. We have calculated the parity-violating asymmetry parameter as it is directly related to the Fourier transform of the neutron density. The evolution of the position of the first diffraction minimum of the asymmetry parameter as a function of the neutron-to-proton asymmetry can provide an alternative source of information on the neutron distribution along each isotonic chain.

ACKNOWLEDGMENTS

This work was partially supported by the Italian MIUR through the PRIN 2009 research project.

-
- [1] R. Hofstadter, *Rev. Mod. Phys.* **28**, 214 (1956).
 - [2] T. W. Donnelly and J. D. Walecka, *Ann. Rev. Nucl. Part. Sci.* **25**, 329 (1975).
 - [3] T. W. Donnelly and I. Sick, *Rev. Mod. Phys.* **56**, 461 (1984).
 - [4] S. Boffi, C. Giusti, and F. D. Pacati, *Phys. Rept.* **226**, 1 (1993).
 - [5] O. Benhar, D. Day, and I. Sick, *Rev. Mod. Phys.* **80**, 189 (2008).
 - [6] H. De Vries, C. W. De Jager, and C. De Vries, *Atom. Data Nucl. Data Tabl.* **36**, 495 (1987).
 - [7] G. Fricke, C. Bernhardt, K. Heilig, L. A. Schaller, L. Schellenberg, E. B. Shera, and C. W. De Jager, *Atom. Data Nucl. Data Tabl.* **60**, 177 (1995).
 - [8] J. Heisenberg and H. P. Blok, *Ann. Rev. Nucl. Part. Sci.* **33**, 569 (1983).
 - [9] S. Boffi, C. Giusti, F. D. Pacati, and M. Radici, *Electromagnetic Response of Atomic Nuclei*, Oxford Studies in Nuclear Physics, Vol. 20 (Clarendon Press, Oxford, 1996).
 - [10] <http://faculty.virginia.edu/qes-archive/index.html>.
 - [11] S. Frullani and J. Mougey, *Adv. Nucl. Phys.* **14**, 1 (1984).
 - [12] M. Bernheim, A. Bussiere, J. Mougey, D. Royer, S. Tarnowski, D. Turck-Chièze, S. Frullani, S. Boffi, C. Giusti, and F. D. Pacati, *Nucl. Phys. A* **375**, 381 (1982).
 - [13] L. Lapikás, *Nucl. Phys. A* **553**, 297 (1993).
 - [14] P. K. A. de Witt Huberts, *J. Phys. G* **16**, 507 (1990).
 - [15] J. M. Udías, P. Sarriguren, E. Moya de Guerra, E. Garrido, and J. A. Caballero, *Phys. Rev. C* **48**, 2731 (1993).
 - [16] J. Gao *et al.* (The Jefferson Lab Hall A Collaboration), *Phys. Rev. Lett.* **84**, 3265 (2000).
 - [17] A. Meucci, C. Giusti, and F. D. Pacati, *Phys. Rev. C* **64**, 014604 (2001).
 - [18] C. Giusti, A. Meucci, F. D. Pacati, G. Co', and V. De Donno, *Phys. Rev. C* **84**, 024615 (2011).
 - [19] G. Co', V. De Donno, P. Finelli, M. Grasso, M. Anguiano, A. M. Lallena, C. Giusti, A. Meucci, and F. D. Pacati, *Phys. Rev. C* **85**, 024322 (2012).

- [20] I. Tanihata, *Prog. Part. Nucl. Phys.* **35**, 505 (1995).
- [21] H. Geissel, G. Müzenberg, and R. Riisager, *Ann. Rev. Nucl. Part. Sci.* **45**, 163 (1995).
- [22] A. Mueller, *Prog. Part. Nucl. Phys.* **46**, 359 (2001).
- [23] T. Suda, K. Maruyama, and I. Tanihata, *RIKEN Accel. Prog. Rep.* **34**, 49 (2001).
- [24] T. Suda, M. Wakasugi, T. Emoto, K. Ishii, S. Ito, K. Kurita, A. Kuwajima, A. Noda, T. Shirai, T. Tamae, H. Tongu, S. Wang, and Y. Yano, *Phys. Rev. Lett.* **102**, 102501 (2009).
- [25] T. Katayama, T. Suda, and I. Tanihata, *Physica Scripta* **T104**, 129 (2003).
- [26] “An International Accelerator Facility for Beams of Ions and Antiprotons”, GSI report 2006, <http://www.gsi.de/GSI-Future/cdr/>.
- [27] http://www.gsi.de/forschung/fair_experiments/elise/index_e.html.
- [28] H. Simon, *Nucl. Phys. A* **787**, 102 (2007).
- [29] A. N. Antonov *et al.*, *Nucl. Instrum. Meth. A* **637**, 60 (2011).
- [30] T. Suda, “A construction proposal of an electron scattering facility for structure studies of short-lived nuclei”, Proposal for Nuclear Physics Experiments at RIBF NP1006 – SCRIT01 (2010).
- [31] T. Suda, T. Adachi, T. Amagai, A. Enokizono, M. Hara, T. Hori, S. Ichikawa, K. Kurita, T. Miyamoto, R. Ogawara, T. Ohnishi, Y. Shimakura, T. Tamae, M. Togasaki, M. Wakasugi, S. Wang, and K. Yanagi, *Progress of Theoretical and Experimental Physics* **2012**, 03C008 (2012).
- [32] E. Garrido and E. Moya de Guerra, *Nucl. Phys. A* **650**, 387 (1999).
- [33] E. Garrido and E. Moya de Guerra, *Phys. Lett. B* **488**, 68 (2000).
- [34] S. N. Ershov, B. V. Danilin, and J. S. Vaagen, *Phys. Rev. C* **72**, 044606 (2005).
- [35] Z. Wang and Z. Ren, *Phys. Rev. C* **70**, 034303 (2004).
- [36] A. N. Antonov, M. K. Gaidarov, D. N. Kadrev, P. E. Hodgson, and E. Moya de Guerra, *Int. J. Mod. Phys. E* **13**, 759 (2004).
- [37] A. N. Antonov, D. N. Kadrev, M. K. Gaidarov, E. Moya de Guerra, P. Sarriguren, J. M. Udías, V. K. Lukyanov, E. V. Zemlyanaya, and G. Z. Krumova, *Phys. Rev. C* **72**, 044307 (2005).
- [38] C. A. Bertulani, *Phys. Rev. C* **75**, 024606 (2007).
- [39] E. Khan, M. Grasso, J. Margueron, and N. Van Giai, *Nucl. Phys. A* **800**, 37 (2008).
- [40] M. Grasso, L. Gaudefroy, E. Khan, T. Nikšić, J. Piekarewicz, O. Sorlin, N. Van Giai, and D. Vretenar, *Phys. Rev. C* **79**, 034318 (2009).
- [41] Y. Chu, Z. Ren, T. Dong, and Z. W. Wang, *Phys. Rev. C* **79**, 044313 (2009).
- [42] X. Roca-Maza, M. Centelles, F. Salvat, and X. Viñas, *Phys. Rev. C* **78**, 044332 (2008).
- [43] X. Roca-Maza, M. Centelles, F. Salvat, and X. Viñas, *Phys. Rev. C* **87**, 014304 (2013).
- [44] T. Dong, Y. Chu, Z. Ren, and Z. Wang, *Phys. Rev. C* **79**, 014317 (2009).
- [45] T. Dong, Z. Ren, and Z. Wang, *Phys. Rev. C* **77**, 064302 (2008).
- [46] J. Liu, Z. Ren, and T. Dong, *Nucl. Phys. A* **888**, 45 (2012).
- [47] T. Dong, Y. Chu, and Z. Ren, *J. Phys. Conf. Ser.* **381**, 012135 (2012).
- [48] A. Meucci, M. Vorabbi, C. Giusti, F. D. Pacati, and P. Finelli, *Phys. Rev. C* **87**, 054620 (2013).
- [49] T. W. Donnelly, J. Dubach, and I. Sick, *Nuclear Physics A* **503**, 589 (1989).
- [50] T. W. Donnelly and R. D. Peccei, *Physics Reports* **50**, 1 (1979).
- [51] C. J. Horowitz, *Phys. Rev. C* **57**, 3430 (1998).
- [52] S. Abrahamyan *et al.* (PREX Collaboration), *Phys. Rev. Lett.* **108**, 112502 (2012).
- [53] C. J. Horowitz, Z. Ahmed, C. M. Jen, A. Rakhman, P. A. Souder, M. M. Dalton, N. Liyanage, K. D. Paschke, K. Saenboonruang, R. Silwal, G. B. Franklin, M. Friend, B. Quinn, K. S. Kumar, D. McNulty, L. Mercado, S. Riordan, J. Wexler, R. W. Michaels, and G. M. Urciuoli, *Phys. Rev. C* **85**, 032501 (2012).
- [54] PREX-II, Proposal to Jefferson Lab PAC 38, <http://hallaweb.jlab.org/parity/prex/prexII.pdf>.
- [55] C. M. Tarbert *et al.*, (2013), arXiv:1311.0168 [nucl-ex].
- [56] “CREX: parity-violating measurements of the weak charge distribution of ^{48}Ca to 0.03 fm accuracy”, Proposal to Jefferson Lab PAC 39, <http://hallaweb.jlab.org/parity/prex>.
- [57] O. Sorlin and M.-G. Porquet, *Phys. Scr.* **T152**, 014003 (2013).
- [58] B. D. Serot and J. D. Walecka, *Adv. Nucl. Phys.* **16**, 1 (1986).
- [59] P. G. Reinhard, *Rep. Prog. Phys.* **52**, 439 (1989).
- [60] P. Ring, *Prog. Part. Nucl. Phys.* **37**, 193 (1996).
- [61] B. D. Serot and J. D. Walecka, *Int. J. Mod. Phys. E* **6**, 515 (1997).
- [62] D. Vretenar, A. Afanasjev, G. Lalazissis, and P. Ring, *Phys. Rept.* **409**, 101 (2005).
- [63] A. Meucci, F. Capuzzi, C. Giusti, and F. D. Pacati, *Phys. Rev. C* **67**, 054601 (2003).
- [64] A. Meucci, C. Giusti, and F. D. Pacati, *Nuclear Physics A* **739**, 277 (2004).
- [65] A. Meucci, C. Giusti, and F. D. Pacati, *Nuclear Physics A* **756**, 359 (2005).
- [66] A. Meucci, J. A. Caballero, C. Giusti, F. D. Pacati, and J. M. Udías, *Phys. Rev. C* **80**, 024605 (2009).
- [67] A. Meucci, J. A. Caballero, C. Giusti, and J. M. Udías, *Phys. Rev. C* **83**, 064614 (2011).
- [68] A. Meucci and C. Giusti, *Phys. Rev. D* **85**, 093002 (2012).
- [69] A. Meucci, C. Giusti, and F. D. Pacati, *Phys. Rev. D* **84**, 113003 (2011).
- [70] A. Meucci, M. B. Barbaro, J. A. Caballero, C. Giusti, and J. M. Udías, *Phys. Rev. Lett.* **107**, 172501 (2011).
- [71] P. Finelli, N. Kaiser, D. Vretenar, and W. Weise, *Nucl. Phys. A* **770**, 1 (2006).
- [72] S. Bogner, R. Furnstahl, and A. Schwenk, *Prog. Part. Nucl. Phys.* **65**, 94 (2010).

- [73] T. Nikšić, D. Vretenar, P. Finelli, and P. Ring, *Phys. Rev. C* **66**, 024306 (2002).
- [74] J. Decharge and D. Gogny, *Phys. Rev. C* **21**, 1568 (1980).
- [75] J. Berger, M. Girod, and D. Gogny, *Nucl. Phys. A* **428**, 23 (1984).
- [76] M. Serra, A. Rummel, and P. Ring, *Phys. Rev. C* **65**, 014304 (2001).
- [77] R. F. Frosch, R. Hofstadter, J. S. McCarthy, G. K. Nöldeke, K. J. van Oostrum, M. R. Yearian, B. C. Clark, R. Herman, and D. G. Ravenhall, *Phys. Rev.* **174**, 1380 (1968).
- [78] J. W. Lightbody, J. B. Bellicard, J. M. Cavedon, B. Frois, D. Goutte, M. Huet, P. Leconte, A. Nakada, P. X. Ho, S. K. Platchkov, S. Turck-Chieze, C. W. de Jager, J. J. Lapikás, and P. K. A. de Witt Huberts, *Phys. Rev. C* **27**, 113 (1983).
- [79] D. Vretenar, P. Finelli, A. Ventura, G. A. Lalazissis, and P. Ring, *Phys. Rev. C* **61**, 064307 (2000).
- [80] C. J. Horowitz, S. J. Pollock, P. A. Souder, and R. Michaels, *Phys. Rev. C* **63**, 025501 (2001).
- [81] O. Moreno, P. Sarriguren, E. Moya de Guerra, J. M. Udías, T. W. Donnelly, and I. Sick, *Journal of Physics: Conference Series* **312**, 092044 (2011).
- [82] B. Bastin, S. Grévy, D. Sohler, O. Sorlin, Z. Dombrádi, N. L. Achouri, J. C. Angélique, F. Azaiez, D. Baiborodin, R. Borcea, C. Bourgeois, A. Buta, A. Bürger, R. Chapman, J. C. Dalouzy, Z. Dlouhy, A. Drouard, Z. Elekes, S. Franchoo, S. Iacob, B. Laurent, M. Lazar, X. Liang, E. Liénard, J. Mrazek, L. Nalpas, F. Negoita, N. A. Orr, Y. Penionzhkevich, Z. Podolyák, F. Pougheon, P. Roussel-Chomaz, M. G. Saint-Laurent, M. Stanoiu, I. Stefan, F. Nowacki, and A. Poves, *Phys. Rev. Lett.* **99**, 022503 (2007).
- [83] O. Sorlin and M.-G. Porquet, *Progress in Particle and Nuclear Physics* **61**, 602 (2008).
- [84] B. G. Todd-Rutel, J. Piekarewicz, and P. D. Cottle, *Phys. Rev. C* **69**, 021301 (2004).
- [85] Y. Chu, Z. Ren, Z. Wang, and T. Dong, *Phys. Rev. C* **82**, 024320 (2010).
- [86] Z. Wang, Z. Ren, and T. Dong, (2013), arXiv:1305.3027 [nucl-th].
- [87] Y. Wang, J. Gu, X. Zhang, and J. Dong, *Chin. Phys. Lett.* **28**, 102101 (2011).
- [88] J. Yao, H. Mei, and Z. Li, *Phys. Lett. B* **723**, 459 (2013).
- [89] A. Meucci, C. Giusti, and F. D. Pacati, *Phys. Rev. C* **64**, 064615 (2001).
- [90] A. Meucci, *Phys. Rev. C* **65**, 044601 (2002).
- [91] M. Radici, A. Meucci, and W. H. Dickhoff, *Eur. Phys. J. A* **17**, 65 (2003).
- [92] F. Capuzzi, C. Giusti, and F. D. Pacati, *Nuclear Physics A* **524**, 681 (1991).
- [93] F. Capuzzi, C. Giusti, F. D. Pacati, and D. N. Kadrev, *Annals of Physics (N.Y.)* **317**, 492 (2005).
- [94] C. Giusti and A. Meucci, *Journal of Physics: Conference Series* **336**, 012025 (2011).
- [95] A. Meucci, C. Giusti, and M. Vorabbi, *Phys. Rev. D* **88**, 013006 (2013), arXiv:1305.5466 [nucl-th].
- [96] R. González-Jiménez, J. A. Caballero, A. Meucci, C. Giusti, M. B. Barbaro, M. V. Ivanov, and J. M. Udías, *Phys. Rev. C* **88**, 025502 (2013).
- [97] Y. Horikawa, F. Lenz, and N. C. Mukhopadhyay, *Phys. Rev. C* **22**, 1680 (1980).
- [98] C. Maieron, T. W. Donnelly, and I. Sick, *Phys. Rev. C* **65**, 025502 (2002).
- [99] E. D. Cooper, S. Hama, and B. C. Clark, *Phys. Rev. C* **80**, 034605 (2009).
- [100] T. de Forest Jr., *Nuclear Physics A* **392**, 232 (1983).